CFD analysis of drag and convective heat transfer of individual body segments for different cyclist positions

Article

5 authors, including:

Thijs Defraeye
Empa - Swiss Federal Laboratories for Materials Science and Technology
125 PUBLICATIONS   **3,038** CITATIONS

SEE PROFILE

Erwin Koninckx
KU Leuven
17 PUBLICATIONS   **819** CITATIONS

SEE PROFILE

Peter Hespel
KU Leuven
199 PUBLICATIONS   **7,997** CITATIONS

SEE PROFILE

Jan Carmeliet
ETH Zurich
376 PUBLICATIONS   **12,210** CITATIONS

SEE PROFILE

Some of the authors of this publication are also working on these related projects:

Project   image analysis and moisture transport in porous media View project

Project   Microscale modelling of water transport View project

CFD analysis of drag and convective heat transfer of individual body segments for different cyclist positions

Thijs Defraeye [a,*], Bert Blocken [b], Erwin Koninckx [c,d], Peter Hespel [d] and Jan Carmeliet [e,f]

[a] *Laboratory of Building Physics, Department of Civil Engineering, Katholieke Universiteit Leuven, Kasteelpark Arenberg 40, 3001 Heverlee, Belgium*
[b] *Building Physics and Systems, Eindhoven University of Technology, P.O. Box 513, 5600 Eindhoven, The Netherlands*
[c] *Flemish Cycling Federation, Globelaan 49/2, 1190 Brussels, Belgium*
[d] *Research Centre for Exercise and Health, Department of Biomedical Kinesiology, Katholieke Universiteit Leuven, Tervuursevest 101, 3001 Heverlee, Belgium*
[e] *Chair of Building Physics, Swiss Federal Institute of Technology Zurich (ETHZ), Wolfgang-Pauli-Strasse 15, 8093 Zürich, Switzerland*
[f] *Laboratory for Building Science and Technology, Swiss Federal Laboratories for Materials Testing and Research (Empa), Überlandstrasse 129, 8600 Dübendorf, Switzerland*

Abstract
This study aims at investigating drag and convective heat transfer for cyclists at a high spatial resolution. Such an increased spatial resolution, when combined with flow-field data, can increase insight in drag reduction mechanisms and in the thermo-physiological response of cyclists, related to heat stress and hygrothermal performance of clothing. Computational fluid dynamics (steady Reynolds-averaged Navier-Stokes) is used to evaluate the drag and convective heat transfer of 19 body segments of a cyclist for three different cyclist positions. The influence of wind speed on the drag is analysed, indicating a pronounced Reynolds number dependency of the drag, where more streamlined positions show a dependency up to higher Reynolds numbers. The drag and convective heat transfer coefficient (CHTC) of the body segments and the entire cyclist are compared for all positions at racing speeds, showing high drag values for the head, the legs and the arms and high CHTCs for the legs, the arms, the hands and the feet. The drag areas of individual body segments differ markedly for different cyclist positions whereas the convective heat losses of the body segments are found to be less sensitive to the position. CHTC-wind speed correlations are derived, in which the power-law exponent does not differ significantly for the individual body segments for all positions, where an average value of 0.84 is found. Similar CFD studies can be performed to assess drag and CHTCs at a higher spatial resolution for applications in other sport disciplines, bicycle equipment design or to assess convective moisture transfer.

1. Introduction

This paper deals with two important aspects of cyclist performance, namely aerodynamic drag and convective heat transfer from the body. Regarding the first aspect, 90% of the total resistance experienced by a cyclist at racing speeds (± 50 km/h in time trials) is caused by aerodynamic drag (Kyle and Burke, 1984), which is mainly related to the position of the cyclist on the bicycle. Many elite cyclists therefore try to optimise their position for drag by means of field tests or wind-tunnel tests. The resulting aerodynamic improvements are however mostly obtained by trial-and-error since usually only information on the overall cyclist drag is available. An alternative technique is computational fluid dynamics (CFD), which has already been applied for drag evaluation in cycling (Defraeye et al., 2010a; Defraeye et al., 2010b; Hanna, 2002; Lukes et al., 2004) and other sport disciplines (Dabnichki and Avital, 2006; Lecrivain et al., 2008; Minetti et al., 2009; Zaïdi et al., 2008; Zaïdi et al., 2010). CFD can provide drag information at a higher spatial resolution, i.e. on individual body segments or bicycle components, which can increase insight in drag reduction mechanisms, especially when combined with the available flow-field data. A detailed overview and background on cyclist drag is given in Defraeye et al. (2010a; 2010b).

The second aspect of this paper, namely convective heat transfer, is required to assess the thermo-physiological response of cyclists, particularly for cyclist performance analysis related to heat stress (Tatterson et al., 2000; Wilson, 2004) and for hygrothermal analysis of clothing. This response is often analysed with thermoregulatory models (Tanabe et al., 2002; Wan and Fan, 2008) or clothing models (Qian and Fan, 2009). These models use

---

empirically-determined convective heat transfer coefficients (CHTCs; W/m^2K) to estimate the convective heat flux at the cyclist's surface ($q_{c,s}$; W/m^2) from the temperature difference between the surface (T_s; K) and the ambient air (T_{ref}; K): CHTC = $q_{c,s}/(T_s-T_{ref})$. Such CHTCs are essential in these models to quantify the (convective) heat exchange of humans with the exterior environment. CHTCs for humans are usually determined by correlations with the wind speed from: (1) experiments on human manikins in a wind tunnel or a climatic chamber by means of calorimetry (Mitchell et al., 1969), surface heat flux measurements (de Dear et al., 1997; Ishigaki et al., 1993) or naphthalene sublimation (Nishi and Gagge, 1970); (2) CFD simulations (Gao and Niu, 2004; Kilic and Sevilgen, 2008; Ono et al., 2008; Sorensen and Voight, 2003). There is still room for improvement regarding these CHTC-wind speed correlations for cyclist applications: (1) The CHTC magnitude and distribution over the body surface are strongly dependent on the flow field around the cyclist, which is determined by the cyclist position and anthropometric characteristics. In the past, mostly a seated or standing person was considered instead of a cyclist; (2) CHTC predictions are dependent on the type of flow, i.e. forced convection at racing speeds in this study. Previous CHTC studies however often focussed on natural or mixed convection since they analysed the microclimate around humans in buildings, urban environments or in vehicles; (3) Apart from studies on effects of cold outdoor windy environments on humans (Shitzer, 2006), most studies on forced convection evaluated CHTCs at relatively low wind speeds (Ishigaki et al., 1993; Mitchell et al., 1969), typically ≤ 5 m/s thus lower than racing speeds; (4) Experiments only provide a limited spatial resolution: thermal manikins with about 15 body segments are mostly used (de Dear et al., 1997). Often, the CHTC is measured at a specific location on a body segment, which is not always representative for the surface-averaged CHTC of the entire segment; (5) Often, due to lack of more detailed information, correlations for cylinders are used to predict CHTCs for cyclists (Wilson, 2004). Based on these arguments, the available CHTC-wind speed correlations are often not applicable for cyclists and/or have a rather limited spatial resolution. In addition, also a large spread is found between different correlations (Shitzer, 2006).

An increased spatial resolution (i.e. of different body segments) for drag predictions and CHTC-wind speed correlations, specifically for cyclists, would be useful for certain applications: (1) More insight in the relation between cyclist drag and his position or the interaction with equipment (e.g. helmet or clothing) can be obtained. This information can be used for example to evaluate the performance of surface roughness elements on clothing (e.g. boundary-layer (s)trips) for drag reduction by boundary-layer control; (2) More detailed CHTC-wind speed correlations can improve the predictive accuracy of models for thermo-physiological response analysis, which could also enhance experimental studies with thermal manikins, which are often controlled by such models. In addition, predictions of convective moisture removal from the body and heat and moisture transport in clothing could be improved since CHTCs are frequently used to quantify convective mass transfer by applying the heat and mass transfer analogy (Chilton and Colburn, 1934).

This study therefore aims at investigating drag and convective heat transfer at a high spatial resolution, i.e. by subdividing the cyclist in several body segments. CFD is considered the most appropriate technique to obtain high spatial resolution data. The drag and CHTCs of the body segments and the entire cyclist are compared for three different cyclist positions. In addition, the influence of wind speed on the drag (Reynolds number effect) is analysed and CHTC-wind speed correlations are derived.

2. Methods
2.1 Numerical model
Three different positions are investigated (Figure 1), namely the upright position (UP, (a)), the dropped position with straight arms (DP, (b)) and the time-trial position (TTP, (c)). A digital model of the cyclist was obtained for every position using a high-resolution 3D laser scanning system (K-Scan, Nikon Metrology, Belgium), capturing the specific anthropometric characteristics of the cyclist (height = 183 cm, weight = 72 kg), and was used for computational modelling. For meshing purposes of the computational cyclist model, surface details were smoothed out to some extent (by manual postprocessing) and the bicycle was not included in the computational model. The cyclist's body surface was subdivided into 19 body segments (Figure 2), which were approximately the same for all three cyclist positions to allow mutual comparison. The virtual cyclist was placed in a computational domain (Figure 3), representing the surrounding environment, where the wind direction was parallel to the bicycle axis. Simulations were carried out at different free-stream wind speeds (U_∞), namely 10-100 km/h (in steps of 10 km/h, where also 55 km/h is included for UP), i.e. forced-convective flow, in order to identify possible Reynolds number effects on the drag (section 3.1) and to obtain CHTC-wind speed correlations (section 3.3). Additional information on the imposed boundary conditions and on the spatial discretisation can be found in Appendix 1.

Note that the approach-flow conditions in this study (i.e. low turbulence intensity and a uniform velocity profile), as also applied in most wind-tunnel experiments on cyclist aerodynamics, are representative for the case where

only the cyclist is moving and where the wind speed of the surrounding air is zero. This situation is typically found in indoor environments (e.g. a velodrome) or in the outdoor environment if there is no wind. If there is wind in the outdoor environment, i.e. atmospheric boundary-layer flow, the drag experienced by the cyclist will be dependent on both the cyclist speed and the wind speed (and wind direction), where also the higher turbulence level will play a role.

2.2 Numerical simulations

When applying CFD, detailed validation with experiments is strongly advised in order to quantify the accuracy of the applied CFD modelling techniques for the specific flow problem. Note however that it is often difficult to obtain the same experimental spatial resolution as in the CFD simulations, e.g. one overall drag force for the cyclist is obtained in wind-tunnel tests. Thereby, intercomparison of experiments and CFD can often not be performed at the same spatial resolution. Recently, Defraeye et al. (2010a, 2010b) performed detailed wind-tunnel measurements on a cyclist (full-scale and scale model), where, apart from drag, also surface pressures were measured on several locations (up to 115) on the cyclist's body. Thereby, detailed data sets were obtained, which were used for CFD validation. They found that with steady Reynolds-averaged Navier-Stokes (RANS), which is much less computationally expensive than large-eddy simulation, sufficiently accurate drag and surface pressure predictions could be obtained. The RANS shear-stress transport k-ω turbulence model (Menter, 1994) showed the best overall performance but also the standard k-ε model (Launder and Spalding, 1972) performed well, if combined with low-Reynolds number modelling (LRNM) to resolve the boundary layer on the cyclist's surface. This k-ε model showed differences with experiments of 11% (full-scale; Defraeye et al., 2010a) and below 5% (scale model; Defraeye et al., 2010b) for drag. Regarding convective heat transfer predictions, the applied k-ε model with LRNM was found to provide accurate CHTC predictions (e.g. Defraeye et al., 2010c). For computational stability reasons, related to the large size of the computational domain, the standard k-ε model is preferred over the shear-stress transport k-ω model in this study. Additional information on the CFD simulations can be found in Appendix 1.

3. Results
3.1 Reynolds number dependency of drag force

Aerodynamic drag is usually quantified by defining a dimensionless drag coefficient (C_D) which relates the drag force (F_D; N) to the frontal area of the cyclist (A; m^2):

$$F_D = AC_D \frac{\rho U_\infty^2}{2} \tag{1}$$

where ρ is the density of air (kg/m^3) and U_∞ is the approach-flow wind speed (m/s). Often, the drag area (AC_D, m²) is reported instead of C_D since it does not require an explicit determination of the frontal area. An important parameter is the Reynolds number at which this drag area is evaluated since a distinct dependency of the flow field and thus of AC_D on the Reynolds number can be found for bluff bodies, especially when they have a quite streamlined shape (i.e. without sharp edges) as these bodies have no fixed boundary-layer separation points (Wilson, 2004).

In order to identify the Reynolds number dependency of the drag area for the present CFD study, the scaled drag areas of the cyclist (i.e. its total drag area) and of its individual body segments are shown in Figure 4 for all three positions as a function of the Reynolds number (Re), with Re = $U_\infty L_{ref}/\nu$. L_{ref} (m) is a length scale characteristic for the flow problem, which is taken equal to 1 m, and ν (m^2/s) is the kinematic viscosity. The drag areas of the cyclist at 100 km/h (Re = 19.10^5) are 0.235 m² (UP), 0.197 m² (DP) and 0.169 m² (TTP). The drag areas from the wind-tunnel tests of Defraeye et al. (2010a, 2010b) are also given in Figure 4, i.e. for full-scale cyclists for the three aforementioned positions and for a scale model (scale 1:2) of a cyclist in the upright position. A length scale (L_{ref}) of 0.5 m is used for the scale model. This wind-tunnel drag area becomes quasi independent of the Reynolds number (differences with maximal Re ≤ 2%) at Re ≈ 7.10^5, corresponding to a full-scale wind speed of about 35 km/h, for all cyclist positions, although a remaining dependency still exists for the TTP. For the CFD simulations however, a clear difference between the different positions can be noticed for the cyclist drag area, where more streamlined positions show a Reynolds number dependency up to higher Reynolds numbers. For UP, DP and TTP, the cyclist drag area becomes quasi Reynolds number independent at Re ≈ $9.5.10^5$, 11.10^5 and > 19.10^5, respectively, corresponding to full-scale wind speeds of about 50 km/h, 60 km/h and > 100 km/h. The less pronounced Reynolds number dependency for the full-scale experiments (Defraeye et al., 2010a), particularly for the TTP, could partially be related to the cyclist's surface roughness (of skin and clothing), since roughness determines the locations of boundary-layer separation. Note that zero roughness was assumed in the CFD simulations (see Appendix 1), as surface roughness could not be specified with the applied boundary-layer modelling approach.

If the individual body segments are considered, most of them show the same Reynolds number dependency as the overall drag of the cyclist, except for certain body parts. The surface "pelvis2" shows a distinct dependency up to high Reynolds numbers for all positions. For the TTP, also other body segments show a pronounced dependency.

3.2 Drag of individual segments
In Figure 5, the drag areas of the individual body segments ($AC_{D,segment}$), relative to the drag area of the cyclist ($AC_{D,cyclist}$), are compared for the different positions at U_∞ = 60 km/h, which is a typical racing speed, where $AC_{D,cyclist}$ = 0.239 m² (UP), 0.193 m² (DP) and 0.149 m² (TTP). Note that for the TTP, a distinct Reynolds number dependency is still present here. The highest drag values are found for the head, the legs and the arms since they compose the major part of the frontal area and since they have a relatively large surface area. Compared to the UP and DP, the TTP clearly shows different relative drag areas for the head, which is higher since this position is more streamlined whereas the head is a rather protruding element here and thus it makes up a large part of the total frontal area; and for the arms, which are lower as they are positioned more horizontally (only lower part) and quite "sheltered" in front of the chest. Due to its less streamlined shape, the upright position clearly shows a higher drag area for the back, due to the larger wake, and chest, due to its larger part in the frontal area. Assessing the drag areas of individual body segments by means of such charts can be very useful for analysis and optimisation of cyclist positions and to evaluate the performance and positioning of roughness elements on clothing.

3.3 CHTC of individual segments
Analogous to Figure 5, the convective heat loss (J/s) and CHTCs of the individual body segments, relative to the overall heat flow and CHTC of the cyclist, are compared for the different positions at U_∞ = 60 km/h in Figure 6 and Figure 7, respectively, where $CHTC_{cyclist}$ = 90.0 W/m²K (UP), 87.8 W/m²K (DP) and 81.9 W/m²K (TTP). Thereby, apart from a lower drag area, the DP and TTP also show a lower convective heat loss and CHTC. In general, high CHTCs are found for the legs (lower parts), the arms, the hands and the feet, whereas less exposed segments (chest, upper part of legs) and segments in the wake zone (back, pelvis3) show smaller CHTCs. Since the convective heat losses (J/s) of the body segments are, apart from the CHTC (J/sm²K), also dependent on the surface area, segments with small CHTCs but a large surface area (e.g. back) can still make up a large part of the overall convective heat loss and vice versa (e.g. hands). Note however that the reported convective heat flows were determined assuming a uniform body surface temperature (see Appendix 1), by which they are not entirely representative for an actual cyclist: in reality, the surface temperatures of different body segments (thus also the convective heat flows) are also dependent on clothing, equipment (e.g. helmet), solar radiation absorption, long-wave radiation, transpiration and heat transport inside the body. The focus of this study was however on determining CHTCs instead of predicting realistic convective heat losses.

The distribution of the convective heat flows and CHTCs over the body segments does not seem to vary significantly for different positions (apart from for the arms for the TTP), indicating that each segment has about the same share in the overall convective heat loss and CHTC of the cyclist for all positions. Note that the variation of drag area of different segments with position was much larger. Also note that segments which have a relatively low drag area (e.g. chest and back for TTP) can still show a relatively large convective heat loss, indicating that drag and convective heat transfer are not necessarily correlated.

The CHTC-wind speed correlations for the cyclist for the different positions are determined using a power-law CHTC-U_∞ correlation, in accordance with forced-convective heat transfer theory:

$$CHTC = AU_\infty^B \qquad (2)$$

where A and B are a coefficient and an exponent, respectively. Note that a certain Reynolds number dependency of the flow field is inherently incorporated in these correlations (see section 3.1). In Figure 8, the CHTC-U_∞ correlations for the individual body segments (only for UP) and for the cyclist (for UP, DP and TTP) are shown as a function of the wind speed. The coefficients and exponents of these correlations (derived for U_∞ in m/s) are given in Table 1 for all positions. Note that all correlation coefficients (R^2) exceeded 0.995, indicating a good correlation.

The exponent does not differ significantly for the individual body segments for each position, where an average exponent of about 0.84 is found, indicating that the correlations all have approximately the same curvature. The variation in magnitude of the CHTC between the individual body segments is thereby mainly determined by the coefficient A. Previous research on CHTCs for human bodies indicated an exponent of about 0.5-0.6, although also values up to 0.8 were reported (de Dear et al., 1997; Shitzer, 2006). Since the focus in these studies was mainly on a lower wind speed range, typically < 5 m/s (= 18 km/h) thus including natural and mixed convective

flows, and for seated or standing humans, a comparison with the forced-convective correlations for cyclists from the present study is not entirely justified.

Note that the obtained drag areas and CHTCs of some body segments can differ to some extent from reality since the bicycle has been omitted from the analysis, but this effect is considered rather limited for the majority of the body segments. Around the pelvis area however, due to the influence of the saddle, the current predictions will be less trustworthy to some extent. Furthermore, the influence of moving legs will also have an impact, which will be addressed in a follow-up study. In Appendix 1, the CHTC distribution over the surface of the cyclist is given for the different positions.

4. Discussion
Compared to experiments, CFD has the significant advantage that a high spatial resolution can be obtained, by which very local information on drag and convective heat transfer is obtained, which allows investigating the influence of (small) adjustments in the cyclist's position or equipment. Although only 19 body segments were considered in this study, which is equivalent to those used for thermal manikins, drag and (surface-averaged) CHTCs can be evaluated at a much higher spatial resolution if required. Moreover, drag and convective heat transfer could also be investigated with CFD in other sport disciplines, such as swimming, ski jumping or bobsleighing. Preferably, field tests or wind-tunnel tests should also be applied complementary to such CFD studies, as some important aspects cannot be captured by CFD only, e.g the cyclist-bicycle locomotion.

Furthermore, the obtained CHTC data could be used to estimate the convective moisture transfer coefficient (CMTC) by using the heat and mass transfer analogy, which can be relevant for thermo-physiological response analysis of humans, for example related to clothing design. Knowledge on CHTCs and CMTCs at lower wind speeds, which can be obtained from the aforementioned correlations, is also relevant, for example during uphill cycling. Apart from convection, (solar) radiation, clothing and the cyclist metabolic rate also play an important role in the thermal heat balance at the cyclist's surface. They are all included in thermoregulatory and clothing models (e.g. Qian and Fan, 2009; Wan and Fan, 2008), which are used to evaluate cyclist performance related to heat stress and hygrothermal design of clothing.

Although the cyclist's surface (skin or clothing) mostly has a very low roughness, future research should focus on accurate modelling of such surface roughness with CFD so its impact on the flow field (boundary-layer transition points) and convective heat transfer (coefficients) can be accounted for more accurately.
Finally, it has to be acknowledged that this study presents the drag areas and CHTCs of individual body segments for a specific cyclist, with specific anthropometric characteristics. These results can thereby differ slightly for other subjects, but the general trends will be similar.

5. Conclusions
In this study, the drag and convective heat transfer of individual body segments of a cyclist were investigated by means of CFD at a high spatial resolution for three cyclist different positions. Such a high spatial resolution, when combined with flow-field data, can increase insight in drag reduction mechanisms and in the thermo-physiological response of cyclists. A pronounced Reynolds number dependency of the drag area was found, where more streamlined positions showed a dependency up to higher Reynolds numbers. High drag areas were found for the head, the legs and the arms. The drag areas of individual body segments differed markedly for different cyclist positions whereas the convective heat losses of the body segments were found to be less sensitive to the position. Especially the legs, the arms, the hands and the feet showed high convective heat transfer coefficients (CHTCs). The exponent of the CHTC-wind speed power-law correlations did not differ significantly for the individual body segments for all positions, where an average exponent of 0.84 is found. Such CFD studies can be useful for bicycle equipment design (e.g. helmet), optimisation of drag-efficient cyclist positions, other sport disciplines and to assess convective moisture transfer, e.g. for clothing design. Especially the assessment of individual body segments showed to provide valuable additional information and will be used in follow-up studies, a.o. for the optimisation of cyclist performance by improving his position and also for hygrothermal optimisation of race suits.

Director of Sport of the Belgian Cycling Federation, for his enduring interest and support to integrate innovation in cycling.

References

Chilton, T.H., Colburn, A.P., 1934. Mass transfer (absorption) coefficients. Industrial and Engineering Chemistry 26 (11), 1183-1187.

Dabnichki, P., Avital, E., 2006. Influence of the position of crew members on aerodynamics performance of a two-man bobsleigh. Journal of Biomechanics 39 (15), 2733-2742.

de Dear, R.J., Arens, E., Hui, Z., Oguro, M., 1997. Convective and radiative heat transfer coefficients for individual human body segments. International Journal of Biometeorology 40 (3), 141-156.

Defraeye, T., Blocken, B., Koninckx, E., Hespel, P., Carmeliet, J., 2010a. Aerodynamic study of different cyclist positions: CFD analysis and full-scale wind-tunnel tests. Journal of Biomechanics 43 (7), 1262-1268.

Defraeye, T., Blocken, B., Koninckx, E., Hespel, P., Carmeliet, J., 2010b. Computational fluid dynamics analysis of cyclist aerodynamics: Performance of different turbulence-modelling and boundary-layer modelling approaches. Journal of Biomechanics 43 (12), 2281-2287.

Defraeye, T., Blocken, B., Carmeliet, J., 2010c. CFD analysis of convective heat transfer at the surfaces of a cube immersed in a turbulent boundary layer. International Journal of Heat and Mass Transfer 53 (1-3), 297-308.

Gao, N., Niu, J., 2004. CFD study on micro-environment around human body and personalized ventilation. Building and Environment 39 (7), 795-805.

Hanna, R.K., 2002. Can CFD make a performance difference in sport?. In: Ujihashi, S., Haake, S.J. (Eds.), The Engineering of Sport 4. Blackwell Science, Oxford, pp. 17-30.

Ishigaki, H., Horikoshi, T., Uematsu, T., Sahashi, M., Tsuchikawa, T., Mochida, T., Hieda, T., Isoda, N., Kubo, H., 1993. Experimental study on convective heat transfer coefficient of the human body. Journal of Thermal Biology 18 (5-6), 455-458.

Kilic, M., Sevilgen, G., 2008. Modelling airflow, heat transfer and moisture transport around a standing human body by computational fluid dynamics. International Communications in Heat and Mass Transfer 35 (9), 1159-1164.

Kyle, C.R., Burke, E.R., 1984. Improving the racing bicycle. Mechanical Engineering 106 (9), 34-45.

Launder, B.E., Spalding, D.B., 1972. Lectures in Mathematical Models of Turbulence, Academic Press, London, England.

Lecrivain, G., Slaouti, A., Payton, C., Kennedy, I., 2008. Using reverse engineering and computational fluid dynamics to investigate a lower arm amputee swimmer's performance. Journal of Biomechanics 41 (13), 2855-2859.

Lukes, R.A., Hart, J.H., Chin, S.B., Haake, S.J., 2004. The aerodynamics of mountain bicycles: The role of computational fluid dynamics. In: Hubbard, M., Mehta, R.D., Pallis, J.M. (Eds.), The Engineering of Sport 5. International Sports Engineering Association, Sheffield.

Menter, F.R., 1994. Two-equation eddy-viscosity turbulence models for engineering applications. AIAA Journal 32 (8), 1598-1605.

Minetti, A.E., Machtsiras, G., Masters, J.C., 2009. The optimum finger spacing in human swimming. Journal of Biomechanics 42, 2188-2190.

Mitchell, D., Wyndham, C.H., Vermeulen, A.J., Hodgson, T., Atkins, A.R., Hofmeyr, H.S., 1969. Radiant and convective heat transfer of nude men in dry air. Journal of Applied Physiology 26 (1), 111-118.

Nishi, Y., Gagge, A.P., 1970. Direct evaluation of convective heat transfer coefficient by naphthalene sublimation. Journal of Applied Physiology 29 (6), 830-838.

Ono, T., Murakami, S., Ooka, R., Omori, T., 2008. Numerical and experimental study on convective heat transfer of the human body in the outdoor environment. Journal of Wind Engineering and Industrial Aerodynamics 96 (10-11), 1719-1732.

Qian, X., Fan, J., 2009. A quasi-physical model for predicting the thermal insulation and moisture vapour resistance of clothing. Applied Ergonomics 40 (4), 577-590.

Shitzer, A., 2006. Wind-chill-equivalent temperatures: regarding the impact due to the variability of the environmental convective heat transfer coefficient. International Journal of Biometeorology 50 (4), 224-232.

Sorensen, D.N., Voigt, L.K., 2003. Modelling flow and heat transfer around a seated human body by computational fluid dynamics. Building and Environment 38 (6), 753-762.

Tanabe, S., Kobayashi, K., Nakano, J., Ozeki, Y., Konishi, M., 2002. Evaluation of thermal comfort using combined multi-node thermoregulation (65MN) and radiation models and computational fluid dynamics (CFD). Energy and Buildings 34 (6), 637-646.

Tatterson, A.J., Hahn, A.G., Martin, D.T., Febbraio, M.A., 2000. Effects of heat stress on physiological responses and exercise performance in elite cyclists. Journal of Sports Science and Medicine 3 (2), 186-193.

Wan, X., Fan, J., 2008. A transient thermal model of the human body-clothing-environment system. Journal of Thermal Biology 33 (2), 87-97.

Wilson, D.G., 2004. Bicycling Science. 3rd Ed. MIT Press, USA.

Zaïdi, H., Fohanno, S., Taiar, R., Polidori, G., 2010. Turbulence model choice for the calculation of drag forces when using the CFD method. Journal of Biomechanics 43 (3), 405-411.

Zaïdi, H., Taiar, R., Fohanno, S., Polidori, G., 2008. Analysis of the effect of swimmer's head position on swimming performance using computational fluid dynamics. Journal of Biomechanics 41 (6), 1350-1358.
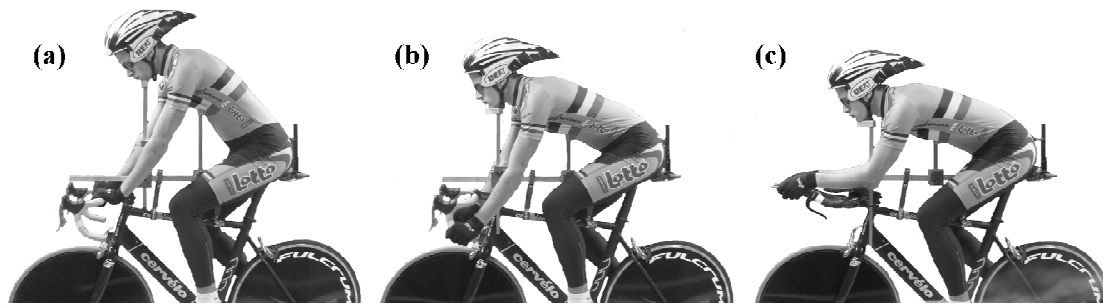
Figure 1. Different cyclist positions: (a) upright position; (b) dropped position; (c) time-trial position.
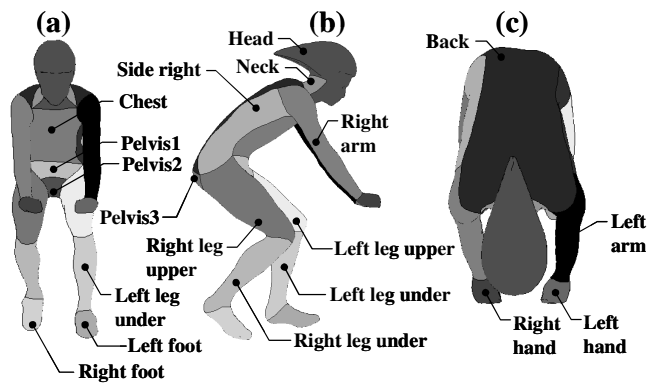
Figure 2. Different body segments of the cyclist, indicated for the upright position: (a) front view; (b) side view; (c) top view.
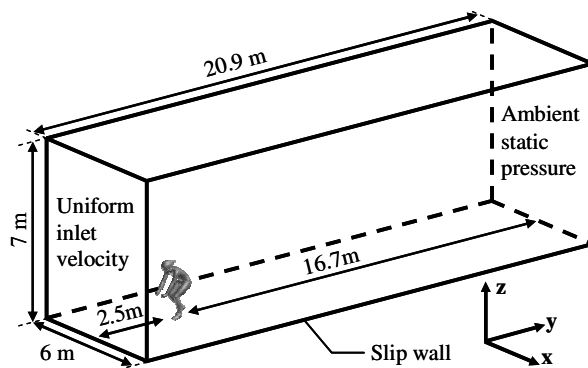

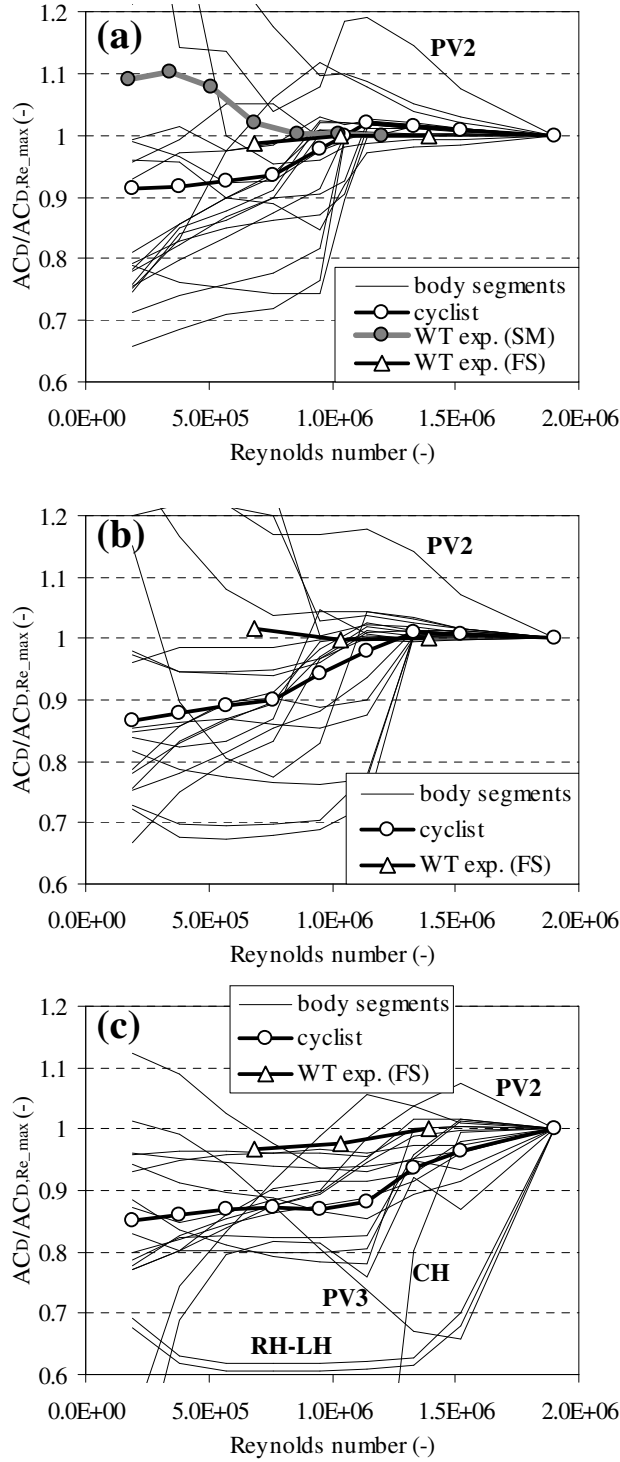**Figure 3. Computational domain and boundary conditions.**

Figure 4. Drag areas from CFD of the cyclist and its individual body segments and from wind-tunnel tests (WT exp. (FS): Defraeye et al., 2010a; WT exp. (SM): Defraeye et al., 2010b, only upright position) as a function of the Reynolds number (based on U_∞ and L_{ref}) for different cyclist positions: (a) upright position; (b) dropped position; (c) time-trial position. The body segments showing strong Reynolds number dependency are indicated (PV2: pelvis2, PV3: pelvis3, CH: chest, RH: right hand, LH: left hand).
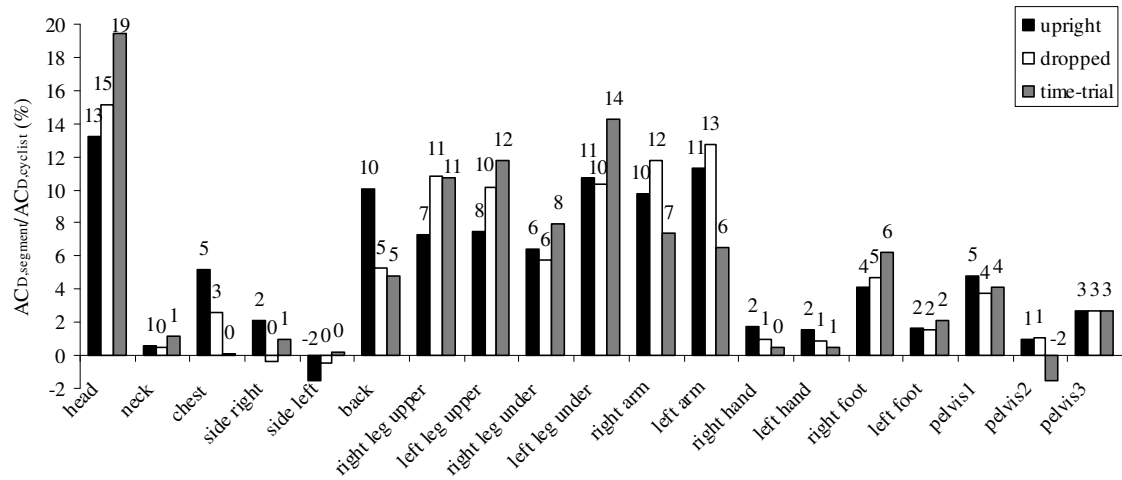
Figure 5. Percentage of drag area of cyclist for the individual body segments (AC$_{D,segment}$/AC$_{D,cyclist}$) for different cyclist positions at U$_\infty$ = 60 km/h.
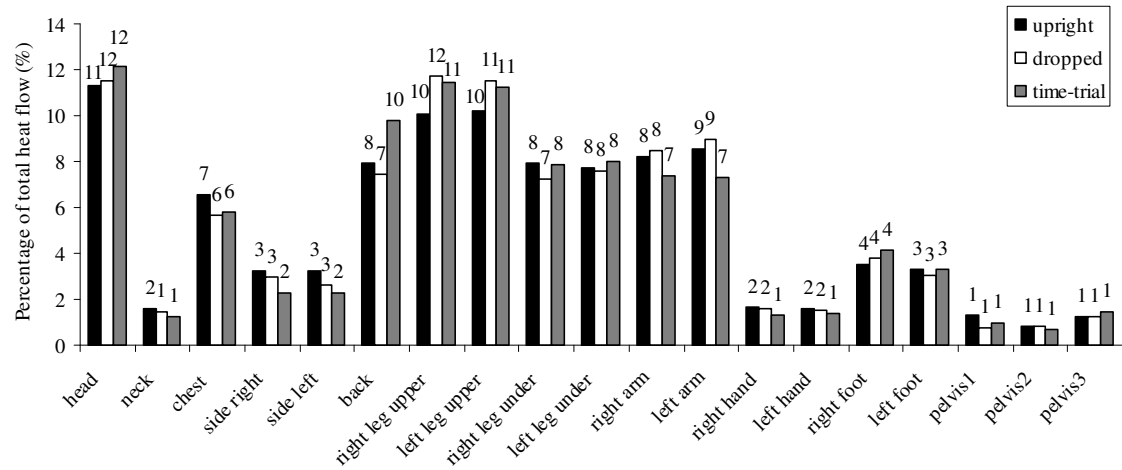

Figure 6. Percentage of overall heat flow from the cyclist's surface for the individual body segments for different cyclist positions at U$_\infty$ = 60 km/h.
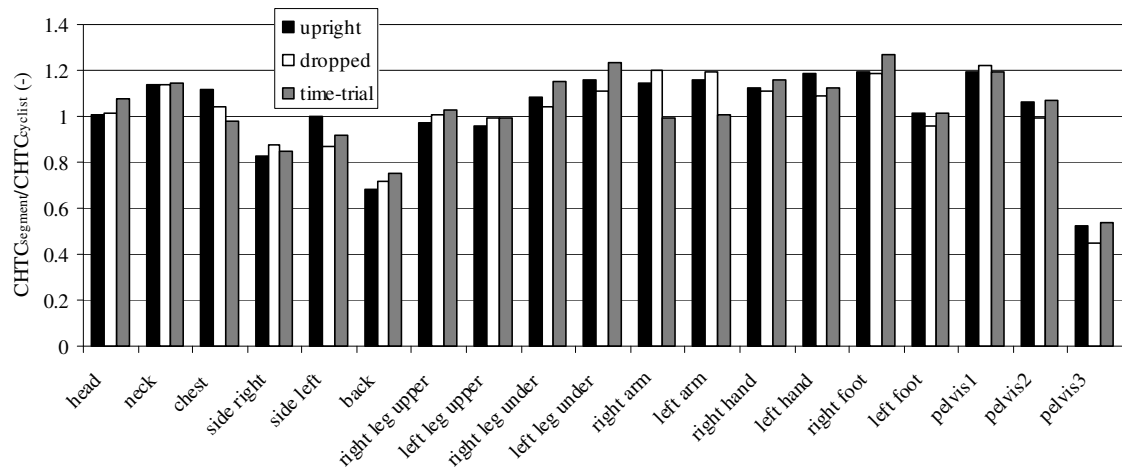

Figure 7. Percentage of overall CHTC of cyclist for the individual body segments (CHTC$_{segment}$/CHTC$_{cyclist}$) for different cyclist positions at U$_\infty$ = 60 km/h.
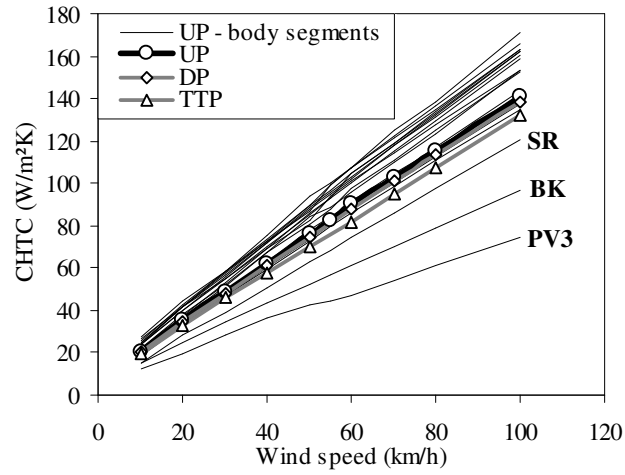
Figure 8. Correlations of CHTC with the wind speed (U∞) for the cyclist (for UP, DP and TTP) and for the individual body segments (only for UP). The body segments which show a low CHTC are indicated (PV3: pelvis3, BK: back, SR: side right).

Tables

Table 1. Coefficient A and exponent B of CHTC-U_∞ correlation (derived for U_∞ in m/s) for the cyclist and for individual body segments for different cyclist positions.

Segment	Upright		Dropped		Time-trial	
	A	B	A	B	A	B
head	8.4	0.85	8.3	0.84	8.3	0.84
neck	9.7	0.84	10.0	0.82	9.6	0.82
chest	8.3	0.88	8.0	0.86	7.5	0.86
side right	5.9	0.90	6.2	0.90	6.2	0.86
side left	7.3	0.90	6.4	0.88	6.3	0.88
back	6.1	0.82	5.7	0.85	5.5	0.87
right leg upper	8.3	0.84	8.2	0.84	8.4	0.83
left leg upper	8.2	0.84	8.1	0.84	8.2	0.82
right leg under	9.2	0.84	9.5	0.82	9.4	0.83
left leg under	9.5	0.85	9.7	0.83	9.7	0.84
right arm	10.3	0.82	10.4	0.82	8.5	0.81
left arm	10.5	0.82	10.4	0.82	8.6	0.81
right hand	11.1	0.78	10.6	0.80	10.8	0.78
left hand	11.7	0.78	10.3	0.81	10.5	0.78
right foot	10.7	0.82	10.3	0.83	10.3	0.82
left foot	9.0	0.82	8.9	0.82	9.2	0.80
pelvis1	9.6	0.86	10.4	0.83	10.7	0.80
pelvis2	8.3	0.87	7.5	0.87	6.9	0.91
pelvis3	5.3	0.79	4.7	0.76	4.8	0.78
cyclist	8.5	0.84	8.4	0.84	8.1	0.83

Supplementary material

Appendix 1

1. Numerical model
Boundary conditions
At the inlet, a low-turbulent, uniform inlet flow was imposed with an approach-flow wind speed U_∞, a turbulence intensity of 0.02% and a temperature (T_{ref}) of 20°C (293.15K). The cyclist's surface was modelled as a no-slip boundary (i.e. a wall) with zero roughness, where a temperature (T_s) of 30°C (303.15K) was imposed. For the side surfaces of the computational domain, a slip-wall boundary (symmetry) was used. Slip walls assume that the normal velocity component and the normal gradients at the boundary are zero, resulting in flow parallel to the boundary. At the outlet of the computational domain, the ambient static pressure was imposed. The maximal blockage ratio was obtained for the upright position and was 1%, which is well below the recommended value of 3% (Franke et al., 2007).

Spatial discretisation
The grid is a hybrid grid, consisting of prismatic cells in the boundary-layer region on the cyclist's surface, tetrahedral elements in the vicinity of the cyclist and hexahedral elements further away from the cyclist, which results in a total amount of $7.3\text{-}7.5.10^6$ computational cells, depending on the cyclist position. The grid was built according to best practice guidelines in CFD (Casey and Wintergerste, 2000), based on a grid sensitivity analysis. The average cell size in the wake region is 0.03 m. The y^+ values on the surface of the cyclist are below 3 for all wind speeds that were evaluated, indicating a high grid resolution in the boundary-layer region, which is required for low-Reynolds number modelling (LRNM).

2. Numerical simulation
The simulations are performed with the CFD code Fluent 12, which uses the control volume method. Steady Reynolds-averaged Navier-Stokes (RANS) is used, namely the standard k-ε turbulence model (Launder and Spalding, 1972) in combination with LRNM to resolve the boundary layer on the cyclist's surface, for which the one-equation Wolfshtein model (Wolfshtein, 1969) is used. Note that surface roughness values cannot be specified since LRNM is used to model the boundary layer. Radiation is not considered since the focus of this study was on determining CHTCs. Since the influence of the temperature dependency of the air properties on the CHTC was found to be limited (Shitzer, 2006), constant air properties are used in this study. Buoyancy is not considered in the simulations since the Richardson number is far below one for cyclists at racing speeds, indicating forced-convective flow. Thereby, the flow field is independent of the thermal boundary conditions, by which their impact on the CHTC is rather limited.

Second-order discretisation schemes are used throughout. The SIMPLE algorithm is used for pressure-velocity coupling. Pressure interpolation is second order. Convergence was assessed by monitoring the velocity and turbulent kinetic energy on specific locations in the flow field and surface friction and heat fluxes on the surface of the cyclist.

Upright position
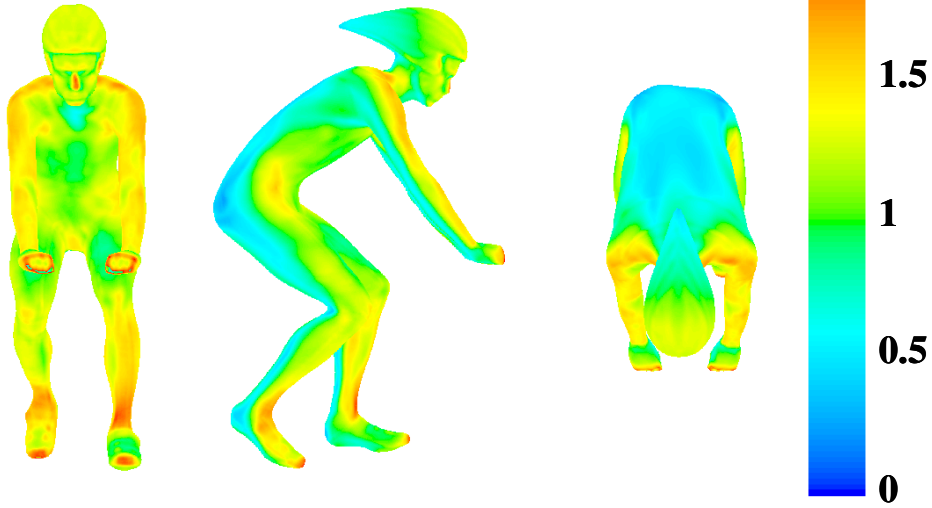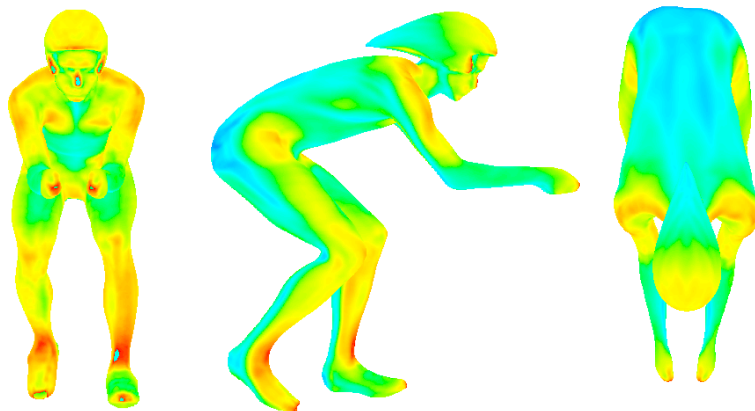

Dropped position
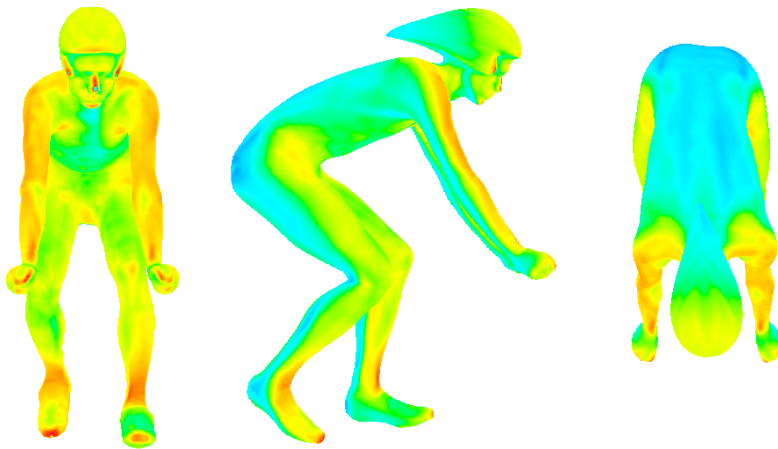
Time-trail position

Figure 1. CHTC distribution on the cyclist's surface for different positions for U_∞ = 60 km/h, made dimensionless with the surface-averaged CHTC of the cyclist ($CHTC_{cyclist}$), for front view, side view and top view.

References

Casey, M., Wintergerste, T., 2000. Best Practice Guidelines. ERCOFTAC Special Interest Group on "Quality and Trust in Industrial CFD", ERCOFTAC.

Franke, J., Hellsten, A., Schlünzen, H., Carissimo, B., 2007. Best practice guideline for the CFD simulation of flows in the urban environment, COST Action 732: Quality assurance and improvement of microscale meteorological models, Hamburg, Germany.

Launder, B.E., Spalding, D.B., 1972. Lectures in Mathematical Models of Turbulence, Academic Press, London, England.

Shitzer, A., 2006. Wind-chill-equivalent temperatures: regarding the impact due to the variability of the environmental convective heat transfer coefficient. International Journal of Biometeorology 50 (4), 224-232.

Wolfshtein, M., 1969. The velocity and temperature distribution in one-dimensional flow with turbulence augmentation and pressure gradient. International Journal of Heat and Mass Transfer 12 (3), 301-318.